Title

An investigation of layer-specific tissue biomechanics of porcine atrioventricular valve anterior leaflets.

Authors

Kramer, Katherine
Ross, Colton
Laurence, Devin
et al.

Publication Date

2019-09-15

DOI

10.1016/j.actbio.2019.06.049

Peer reviewed

Published in final edited form as:
Acta Biomater. 2019 September 15; 96: 368–384. doi:10.1016/j.actbio.2019.06.049.

An investigation of layer-specific tissue biomechanics of porcine atrioventricular valve anterior leaflets

Katherine E. Kramer[a], **Colton J. Ross**[a], **Devin W. Laurence**[a], **Anju R. Babu**[a,1], **Yi Wu**[a], **Rheal A. Towner**[b], **Arshid Mir**[c], **Harold M. Burkhart**[d], **Gerhard A. Holzapfel**[e,f], **Chung-Hao Lee**[a,g,*]

[a]Biomechanics and Biomaterials Design Laboratory, School of Aerospace and Mechanical Engineering, The University of Oklahoma, Norman, OK 73019, USA

[b]Advanced Magnetic Resonance Center, MS 60, Oklahoma Medical Research Foundation, Oklahoma City, OK 73104, USA

[c]Division of Pediatric Cardiology, Department of Pediatrics, University of Oklahoma Health Sciences Center, Oklahoma City, OK 73104, USA

[d]Division of Cardiothoracic Surgery, Department of Surgery, University of Oklahoma Health Sciences Center, Oklahoma City, OK 73104, USA

[e]Institute of Biomechanics, Graz University of Technology, Graz, Austria

[f]Department of Structural Engineering, Norwegian University of Science and Technology (NTNU), Trondheim, Norway

[g]Institute for Biomedical Engineering, Science and Technology, The University of Oklahoma, Norman, OK 73019, USA

Abstract

Atrioventricular heart valves (AHVs) are composed of structurally complex and morphologically heterogeneous leaflets. The coaptation of these leaflets during the cardiac cycle facilitates unidirectional blood flow. Valve regurgitation is treated preferably by surgical repair if possible or replacement based on the disease state of the valve tissue. A comprehensive understanding of valvular morphology and mechanical properties is crucial to refining computational models, serving as a patient-specific diagnostic and surgical tool for preoperative planning. Previous studies have modeled the stress distribution throughout the leaflet's thickness, but validations with layer-specific biaxial mechanical experiments are missing. In this study, we sought to fill this gap in literature by investigating the impact of microstructure constituents on mechanical behavior throughout the thickness of the AHVs' anterior leaflets. Porcine mitral valve anterior leaflets

*Corresponding author at: School of Aerospace and Mechanical Engineering, Affiliated Faculty Member, Institute for Biomedical Engineering, Science, and Technology, The University of Oklahoma, 865 Asp Ave., Felgar Hall Rm. 219C, Norman OK 73019-3609, USA., ch.lee@ou.edu (C.-H. Lee).
[1]Present Affiliation: Department of Biotechnology and Medical Engineering, National Institute of Technology Rourkela, Rourkela, Odisha 769008, India.

Declaration of Competing Interest
None.

Appendix A. Supplementary data
Supplementary data to this article can be found online at https://doi.org/10.1016/j.actbio.2019.06.049.

(MVAL) and tricuspid valve anterior leaflets (TVAL) were micro-dissected into three layers (atrialis/spongiosa, fibrosa, and ventricular) and two layers (atrialis/spongiosa and fibrosa/ventricularis), respectively, based on their relative distributions of extracellular matrix components as quantified by histological analyses: collagen, elastin, and glycosaminoglycans. Our results suggest that (i) for both valves, the atrialis/spongiosa layer is the most extensible and anisotropic layer, possibly due to its relatively low collagen content as compared to other layers, (ii) the intact TVAL response is stiffer than the atrialis/spongiosa layer but more compliant than the fibrosa/ventricularis layer, and (iii) the MVAL fibrosa and ventricularis layers behave nearly isotropic. These novel findings emphasize the biomechanical variances throughout the AHV leaflets, and our results could better inform future AHV computational model developments.

Keywords

Biaxial mechanical testing; The mitral and tricuspid valves; Valve tissue biomechanics; Morphological analysis; Micro-dissection; Extracellular matrix

1. Introduction

Atrioventricular heart valves, also known as the mitral valve (MV) and the tricuspid valve (TV), are situated between the heart's atrial and ventricular chambers and regulate the unidirectional blood circulation through the heart. Considered a bicuspid valve, the MV is composed of an anterior leaflet (AL) and a posterior leaflet (PL). The TV is aptly named for its three-leaflet structure: AL, PL, and septal leaflet (SL). The MV facilitates blood flow through the left side of the heart, and the TV functions likewise on the right side of the heart. These valves, when healthy, prevent pernicious backflow of blood from the ventricle into the atrium, whereas retrograde flow may occur in diseased valves, known as *valve regurgitation.* More than 5 million Americans each year are diagnosed with moderate to severe valvular heart disease [1,2], and each patient has a unique clinical history and varied anatomy, which lends itself to the need for patient-specific treatment options. Standard heart valve therapies have approached many cases as congruous, while additionally failing to recognize the functional importance of the 'forgotten' tricuspid valve [3–6]. Recent studies have refuted such practices, inciting researchers and clinicians to acknowledge the need for a more comprehensive understanding of valvular disease etiology, specifically regarding the right-sided heart valve disease [3,7].

From the anatomical/microstructural perspectives, the MV and TV leaflets—composed of an extracellular matrix (ECM) and valvular interstitial cells (VlCs)—organize into four morphologically-distinct layers: atrialis (A), spongiosa (S), fibrosa (F), and ventricularis (V). The atrialis and ventricularis layers are defined by their outward surface with respect to the atrial and ventricular chambers. Enclosed within these outer layers are the hydrated spongiosa layer, nearest the atrialis, and the collagenous fibrosa layer [8–10]. The microstructural heterogeneity allows for the layers to be histologically identified. Histological evaluation has shown the fibrosa layer to be primarily comprised of Type I collagen fibers. The fibrosa's dense network of crimped collagen fibers is predominantly aligned in a circumferential direction, which contributes to the leaflet tissue's load-bearing

capacity in response to physiological stresses. As the leaflet undergoes loading during cardiac function, the crimped fibers unfold, straighten, and elongate, providing the tissue fiber-reinforced stiffening. The marked difference in the stiffness between the circumferential and radial directions is known as material anisotropy. In contrast to the other layers, the spongiosa is composed of hydrated glycosaminoglycans (GAGs) and proteoglycans (PGs). This layer has been hypothesized to function as a lubricant between the atrialis and fibrosa as the leaflets experience shearing during systole and diastole, but its function has yet to be fully understood [11,12]. The ventricularis layer, composed of collagen and elastin fibers, serves as an insertion point for the chordae tendineae that anchor the leaflets to the papillary muscles [13]. The elastin fibers, present in both the atrialis and ventricularis layers, facilitate leaflet movement and restoration to its undeformed geometry after loading.

Diagnoses of valvular diseases are typically made using noninvasive imaging modalities, such as echocardiography and magnetic resonance imaging (MRI), that provide a comprehensive visualization of the anatomical structure and fluid flow in real time [14]. While imaging technologies have radically enhanced valvular disease diagnoses and treatment options, patient-specific computational models offer yet another potential for preoperative planning. Present efforts have focused on finite element simulations and incorporating image-based patient data to preoperatively examine the effect of surgical remodeling on leaflet stress and function [15–19]. Such high-fidelity models integrate constitutive parameters based on soft tissue material properties, valvular microstructure, and heterogeneous organization, generally obtained from bulk tissue experimental data [10,20–27]. Substantial advancements have been made in refining such computational models, although essential gaps in knowledge persist. While layer-specific models based on ECM distribution exist for the aortic valve [28,29], limited layer-specific modeling work is found in literature for the atrioventricular valve leaflets. Mitral valve constitutive models considered in previous studies utilized layer-specific parameters to investigate microstructural contribution to the bulk tissue function, but these models lacked experimental values to corroborate their findings [30,31].

Thus, the overall objective of this study is to fill this knowledge gap in layer-specific mechanical behaviors and characterize the structure-function relationship of the TV and MV tissue layers using biaxial mechanical testing and histology. In this study, the anterior leaflet was selected as a representative leaflet for both the MV and the TV because of its relatively larger thickness compared to the other atrioventricular leaflets (MVAL: 0.79 mm, MVPL: 0.70 mm; TVAL: 0.52 mm, TVPL: 0.46 mm, TVSL: 0.37 mm [10]), thus making micro-dissection more feasible. For biaxial testing of individual leaflet layers, a micro-dissection protocol was devised to separate porcine TVALs and MVALs into two and three distinct layers, respectively. Force-controlled biaxial mechanical testing with various loading ratios was performed on the separated layers to investigate the mechanical response and coupling behaviors of each tissue layer. The observed layer-specific biomechanical properties were collated with the results of biaxial mechanical testing of intact bulk regions of leaflet tissues, as performed in our previous study [10]. The results of this study will provide a useful quantification of tissue mechanics for each individual leaflet layer to be used in the future development of AHV-specific constitutive models.

2. Methods

2.1. Tissue preparation

Porcine hearts (1–1.5 years of age, 80–140 kg of weight, n = 6) were obtained from a local USDA approved abattoir (Country Home Meat Company, Edmond, OK) to examine the mechanical properties of morphologically-distinct layers of the atrioventricular valve leaflets. The fresh tissues were transported on ice and stored in the laboratory freezer within 12 h post-mortem. The hearts were later thawed to excise the MVAL and TVAL from their respective chambers. The dissected leaflets (Fig. 1a) were preserved in a standard –14 °C freezer for a maximum of two weeks. Freezing was employed based on previous studies that have shown in practice to induce negligible degradation of skin and arterial tissues over short-duration storage [11,32].

2.2. Micro-dissection of atrioventricular valve leaflet tissues

2.2.1. Valve leaflet layers for separation—To sustain high transvalvular pressure loading, the MVAL is distinctly thicker than the TVAL [10,33]. The varied physiological requirements of the leaflets are manifested morphologically in the leaflet percent content of collagen (MVAL: ~77%; TVAL: ~68%). The difference in the collagen content, together with the thickness disparity, proved attaining a testable TVAL ventricularis specimen to be implausible. Thus, only two layers (A/S: combined atrialis-spongiosa layer; F/V: combined fibrosa-ventricularis layer) were segmented for the TVAL, whereas separating the MVAL into three tissue layers (A/S: atrialis/spongiosa; F: fibrosa; V: ventricularis) was possible.

2.2.2. Layer separation procedure—Preceding biaxial mechanical testing, the leaflet was thawed at room temperature in phosphate-buffered saline (PBS) solution, and tissue thickness measurements were taken via a digital caliper (Westward Tools) from 3 different locations and averaged to obtain a representative thickness for the full, intact leaflet. The microdissection technique for separating MVAL and TVAL tissue layers was based on previously developed protocols for the aortic valve, as modified to be efficaciously integrated with our laboratory equipment and leaflets of interest [11,34]. In brief, an intact leaflet was mounted on a wax dissecting pan (American Educational Products LLC), oriented with the atrialis facing upwards. The perimeter of the leaflet was stretched tautly and fastened to the tray with six 9/16” head T-pins (Eisco Labs). Once secured, two delicate incisions (practicing extreme caution so as not to penetrate deeper than the uppermost layer) were made along the leaflet’s central belly region, known as the clear zone (Fig. 1a–c). Dissecting forceps were used to gently pull against the severed atrialis/spongiosa, exposing the fibrillar interconnections bisecting the atrialis and fibrosa. These chords, contained within the spongiosa, were trimmed using ophthalmic scissors. Obtainment of a ~4 × 4 mm section prompted the detachment of the layer from the remaining bulk tissue. To perform the MVAL ventricularis micro-dissection, the tissue was flipped (ventricularis-up) and remounted to the tray. The initial procedure was repeated. After the MVAL/TVAL atrialis/spongiosa, and the MVAL ventricularis layer was further removed, a square specimen of the exposed fibrosa was excised from the bulk leaflet. Additionally, a strip of an intact tissue (~2 × 0.5 mm), from above the dissected region (Fig. 1b) was removed and stored as a baseline for histological comparison. The average thickness of each separated layer was determined

from caliper-measurements at 3 locations. Tissue hydration was maintained throughout the micro-dissection process by periodically moistening the leaflet with PBS. After each specimen was obtained, the radial direction of the tissue was marked using a surgical pen to ensure proper tissue alignment with respect to the biaxial testing's orientations in the subsequent mechanical testing.

2.3. Biaxial mechanical testing

The mechanical properties of each separated tissue layer of the MV and TV were characterized using a commercial biaxial mechanical testing system (BioTester, CellScale Biomaterials Testing, Canada). A square section of the separated tissue layer was obtained from the clear zone (n = 6) and mounted onto the BioTester system equipped with 1.5 N load cells (Fig. 2a and b). Tissue specimens were approximately 4 × 4 mm in size with an effective testing region of approximately 3.5 × 3.5 mm delimited by the tines of 4 BioRakes. Four fiducial markers were made by a surgical pen in a square array for later optical tracking of tissue deformation (Fig. 2a). The sample was then submerged in PBS and warmed to physiological temperature (37 °C). For force-controlled biaxial mechanical testing, procedures developed in our previous work were employed [10]. The testing protocol consisted of eight preconditioning cycles with a preload of 2.5% of the peak membrane tension to restore the tissue to its *in vivo* functional state, followed by five different force loading ratios of the targeted peak membrane tension ($T_{circ,max}$:$T_{rad,max}$ = 1:1, 0.75:1, 1:0.75, 0.5:1, 1:0.5, Fig. 2c), at a loading rate of 2.29 N/min, to elucidate the layer's mechanical behavior under various deformation states. Here, $T_{circ,max}$ and $T_{rad,max}$ are the maximum membrane tensions in the tissue's circumferential and radial directions, respectively, which were calculated based on each atrioventricular valve's physiological pressure gradient, i.e., 100 mmHg for the MV and 40 mmHg for the TV [20,24,35], and the tissue's specimen size. For this calculation, the targeted *in vivo* leaflet stress value was first approximated using Laplace's law for a spherical surface with a 2 cm radius of curvature arriving at 255 kPa for the MV and 115 kPa for the TV [10], respectively. Then, this stress value was multiplied by the average thickness of the *bulk* valve leaflet acquired in our previous study [10] to determine the targeted membrane tension.

After completion of the five tension loading ratios, an equibiaxial tension protocol was performed to examine the repeatability of the stress-stretch curves to ensure that no damage occurred throughout the testing. Throughout testing, a high-resolution CCD camera (The Imaging Source LLC, Charlotte, NC) was used to capture a series of 1280 × 960 images for determining the tissue stretches based on a digital image correlation (DIC) procedure (Fig. 2d). Details of this DIC method can be found in our previous work [10,21].

2.4. Tissue stress-stretch calculations

For more details on the tissue stress and stretch calculations, refer to our previous study. In short, DIC functions in the LabJoy software of the BioTester system were used to obtain the time-dependent locations of the four fiducial markers. Marker locations were used to compute the deformation gradient **F**. From the deformation gradient, tissue stretch values were obtained as the square root of the principal values of the right Cauchy-Green tensor **C**. Membrane tension T was derived through the load cell force reading f of the BioTester, and

the edge length L of the tissue's testing region: $diag[T_{circ}, T_{rad}] = diag[f_{circ}, f_{rad}]/L$. Membrane tension values may be translated to stress measures using the average specimen thickness t, which was measured prior to any mechanical testing. Some examples include, the first Piola-Kirchhoff stress, $\boldsymbol{P} = diag[P_{CC}, P_{RR}] = diag[T_{circ}, T_{rad}]/t$; the second Piola-Kirchhoff stress, $\boldsymbol{S} = \boldsymbol{F}^{-1}\boldsymbol{P}$; and the Cauchy stress, $\boldsymbol{\sigma} = \boldsymbol{J}^{-1}\boldsymbol{P}\boldsymbol{F}^{T}$.

As in our previous study [10], the peak tissue stretches (λ_{circ}^{0-peak} and λ_{rad}^{0-peak}), which were tissue stretches at the peak membrane tensions with respect to the tissue unmounted configuration (Ω_0), were decomposed into two parts for better comparison of tissue material behaviors: (i) *preconditioning stretches* (λ_{circ}^{0-1} and λ_{rad}^{0-1}), which were tissue stretches observed at the end of the preconditioning protocol as determined between configuration Ω_0 and the post-preconditioning configuration (Ω_1), and (ii) *mechanical stretches* (λ_{circ}^{1-peak} and λ_{rad}^{1-peak}), which were defined as the tissue stretches at the peak membrane tensions with respect to the post-preconditioning configuration (Ω_1). The peak tissue stretches are related to the preconditioning and mechanical stretches by

$$\lambda_{circ}^{0-peak} = \lambda_{circ}^{1-peak} \times \lambda_{circ}^{0-1} \text{ and } \lambda_{rad}^{0-peak} = \lambda_{rad}^{1-peak} \times \lambda_{rad}^{0-1} \quad (1)$$

This stretch decomposition is used to allow for direct comparisons of the preconditioning effects between tissue samples, as well as for comparisons of the mechanical responses beyond preconditioning which would be equivalent to the *in vivo* functioning condition. To compare layer-specific material anisotropy, an anisotropy index (AI) was calculated defined as the ratio of peak tissue stretch in the radial direction to the circumferential direction: $AI = \lambda_{rad}^{0-peak}/\lambda_{circ}^{0-peak}$.

2.5. Histology

To confirm the accuracy of the employed micro-dissection method and to quantify the tissue's microstructure, histology was used. This histological evaluation is consistent with the limited existing comparable studies on the aortic valve leaflets [11]. The separated MVAL and TVAL tissue layers and the intact tissue strip were acquired via the standard dissection technique developed in the laboratory (cf. Section 2.2). All tissues were fixed in 10% formalin at room temperature (23 °C), embedded in paraffin wax, and sectioned (5–7 μm). Movat's pentachrome stain was selected based on its ability to reveal comprehensive information about the microstructural organization: elastin stains *purple*, collagen stains *yellow,* and ground substance stains *blue.* The stained sections were viewed under a halogen illumination microscope (Olympus) at a 4× magnification for the intact layers and a 10× magnification for the separated layers. A single image was acquired from each stained tissue. The microstructural ECM components—collagen, elastin, and ground matrix substance—were quantified by volume in accordance with previous studies [8,36] utilizing the ImageJ (National Institute of Health) color deconvolution method [36,37]. For each histological image, three measurements of the tissues' thickness and constituent percentages were made and analyzed. These three measurements were then averaged. It is noted that the

tissue strip analyzed for the intact MVAL/TVAL was a different tissue strip from the layer-separated tissue but was still from the same leaflet tissue (cf. Fig. 1b).

2.6. Statistical analysis

For statistical analyses, each data set was first individually visualized on a quantile-quantile (Q-Q) plot to observe the normality of the experimental data (Figs. S1–S5). These Q-Q plots generally showed a linear relationship when comparing the experimental data to the normal distribution, but there were quite a few cases with an outlier from this relationship. Thus, the non-parametric Mann-Whitney U test was used to determine statistical differences, rather than the one-way Analysis of Variance (ANOVA). Comparisons were made between the decomposed stretch values in the circumferential and radial directions for determining statistically-significant mechanical responses. Furthermore, comparisons of the peak stretch, preconditioning stretch, mechanical stretch, and the anisotropy index were made between different layers within the same AHV to determine statistically-significant differences in the layer-specific mechanical responses. In all statistical analyses, the value of $p < 0.05$ was considered as *statistically significant* and $p < 0.1$ as *nearly statistically significant.*

3. Results

3.1. Leaflet tissue layer separation

Histology confirmed the successful separation of distinct layers in their entirety for both the MVAL (Fig. 3a and b) and the TVAL (Fig. 3c and d) via our micro-dissection technique. Accordingly, the atrialis was shown to be bisected from the fibrosa layer within the spongiosa layer for both leaflets, and the non-fibrous ground substance of the severed spongiosa remained largely intact with the separated atrialis. As such, we considered the thin upper layer to be the atrialis/spongiosa (A/S) layer (Fig. 3b and d). For mechanical testing of the TVAL specifically, the denser bottom layer was considered a combined fibrosa/ventricularis (F/V) layer (Fig. 3d). The MVAL ventricularis could be further separated from the fibrosa layer, with the partition occurring at the cusp of the two layers (Fig. 3b). From the histological results, we determined that the manually performed micro-dissection did not induce any discernible tissue damage.

3.2. Microstructural component quantification

The percent composition for each separated layer as well as the intact leaflets are presented in Tables 1 and 2. Histological image-based microstructural quantification indicated both the MV and TV anterior leaflets to be primarily composed of circumferentially-oriented collagen fiber networks (Fig. 3a and c). The total GAG composition of the intact leaflets was greater than the total elastin composition in the TVAL and MVAL (27.4% and 22.4%, respectively). Additionally, elastin fibers constituted a similar percentage of the TVAL (elastin: 14.3%, collagen: 58.3%) to the MVAL (elastin: 14.8%, collagen: 62.8%), but the MVAL was more collagenous. Both the TVAL-A/S and F/V layers contained only a small fraction of ground substance. The elastin struts in the fibrosa and ventricularis appear to be radially-oriented (Fig. 3b and d) while the atrialis displays a more complex, random alignment of elastin fibers (Fig. 3a and c). This observation suggests a characteristic structure-mechanics-function relationship between the elastic atrialis and its facilitation of

valve motion during cardiac function, which was previously reported for the functional interactions between the fibrosa and the ventricularis of aortic valve leaflets [38].

3.3. Biaxial mechanical testing results

3.3.1. Responses of TVAL layers—Biaxial mechanical testing data of the representative TVAL layer specimens subject to five different loading ratios ($T_{circ,max}$: $T_{rad,max}$ = 1:1, 0.75:1, 1:0.75, 0.5:1, and 1:0.5) are presented in Fig. 4a and b. The nonlinear, anisotropic mechanical behaviors of both TVAL A/S and F/V layers were identified from the peak tissue stretch (Fig. 5a–e, Table 3), showing the A/S and F/V layers to be 9.0% (p = 0.132) and 12.3% (p = 0.310) more extensible in the radial direction than in the circumferential direction, respectively. The anisotropy largely stems from the specimen's preconditioning stretch (Table 3, Fig. 6a and b) as separated from the peak tissue stretch. The average preconditioning stretch in the radial direction was 0.11 greater (p = 0.132) for the A/S and 0.14 greater (p = 0.093) in the F/V than the respective circumferential preconditioning stretch (Table 3, Fig. 6b). Interestingly, the mechanical stretches, decomposed from the tissue stretches, for TVAL layers were found to be nearly isotropic, independent of the loading protocol (Table 4, Fig. 7a–e). Table 5 provides a summary of the statistical analyses comparing the stretches in the circumferential and radial directions.

Additionally, the tissue stretches of the A/S layer and F/V layer revealed the A/S to be more compliant under all loading ratios (p = 0.240–0.589) (Table 3, Fig. 5a–e). This observation was manifested in the apparent toe region for the A/S layer, as compared to the abrupt transition from a low to a high modulus for the F/V. In comparison to the intact TVAL as investigated in our previous studies [10,27], the tissue stress-stretch curve of the intact TVAL was fully encompassed within the ranges between the A/S layer (as the upper bounds) and the F/V layer (as the lower bounds). Further, the preconditioning stretches of the intact TVAL tissue fell between the two separated layers in the circumferential direction (Fig. 6a) but were greater than those of the separated layers in the radial direction (Fig. 6b).

From statistical analyses, the TVAL was found to have no significant differences in regard to layer mechanics. An interesting trend was noticed in the statistical analyses of the equibiaxial loading protocol ($T_{circ,max}$:$T_{rad,max}$ = 1:1), namely the TVAL-A/S and TVAL-F/V showed the smallest p-values when comparing differences in the circumferential and radial preconditioning stretches (p = 0.310 and p = 0.329, respectively), and the circumferential and radial peak tissue stretches (p = 0.310 and p = 0.310, respectively) (Tables 3 and 4). Similar trends in statistical significance were observed for the non-equibiaxial loading ratios.

3.3.2. Responses of MVAL layers—Biaxial mechanical testing results of representative MVAL layer specimens are presented in Fig. 4c–e. The tissue stretches of the A/S layer exhibited a nonlinear and anisotropic behavior (Table 3), whereas both the fibrosa and ventricularis layers were found to be more isotropic (Fig. 8a–e). More specifically, the peak tissue stretch in the radial direction $\left(\lambda_{rad}^{0-peak}\right)$ for the A/S was, on average, 6.1% greater (p = 0.699) than that in the circumferential direction (Table 3). In contrast, the difference between the radial and the circumferential stretches for the fibrosa and the

ventricularis layers were marked by a 1.3% ($p = 0.589$) and 1.2% ($p = 0.589$) average increase, respectively (Table 3). The anisotropy of the A/S layer and the isotropy of the F and V layers can be explained by the associated preconditioning and mechanical stretch results. The average preconditioning radial-circumferential stretches differed by 0.08 ($p = 0.394$) for the atrialis/spongiosa but only by 0.02 for both the fibrosa ($p = 0.699$) and the ventricularis ($p = 0.818$) (Table 3, Fig. 6c and d). Moreover, the mechanical stretch results showed that the behavior of the layers after preconditioning is nearly isotropic (Fig. 9a–e). The only layer that marginally diverged from this trend was the ventricularis under non-equibiaxial loading protocols. Table 5 provides a summary of the statistical analyses comparing the stretches in the circumferential and radial directions.

Another key trend observed was the compliant nature of the separated A/S layer, as indicated by the extended toe region (Fig. 8a–e). The fibrosa and ventricularis layers, instead, transitioned from low-to-high stress in a more distinctly linear manner. Relative to the intact MVAL, none of the layers were found to be as extensible in the radial direction. However, the peak tissue stretches of the MVAL A/S and F layers were most closely in agreement with the intact MVAL's peak tissue stretches in the circumferential direction.

From statistical analyses, significant differences in the layer mechanics were observed for the MVAL. Specifically, more significant differences between layers were observed in the equibiaxial loading condition ($T_{circ,max}$:$T_{rad,max}$ = 1:1) for the radial preconditioning stretch ($0.10 < p < 0.59$), circumferential mechanical stretch ($0.07 < p < 0.14$), and radial mechanical stretch ($0.18 < p < 0.40$) (Tables 2–4). Similar trends in statistical significance were observed for the non-equibiaxial loading ratios.

4. Discussion

4.1. Overall findings

The material behaviors of the separated layers were examined within the context of each respective valve leaflet, as well as in comparison to the behavior of the previously documented bulk leaflet mechanical properties [10,20,22–24,26,39]. Despite the relatively small number of specimens tested in this study (n = 6), as compared to our previous investigation (n = 10), the variances in the stretch values (~19% vs. 15–16%) were comparable between these two studies, suggesting that the observed trends would remain consistent considering a large sample size. The present study highlights the subtle and considerable heterogeneity in the tissue biomechanics distributed throughout the intact tissue. Not only did we observe a diverse organization throughout the intact specimen, the distribution of microstructure between the two atrioventricular valve leaflets also varied, likely owing to different transvalvular pressure gradients. As such, a comprehensive understanding of the mechanical role played by ECM components is crucial for high-fidelity computational modeling of the leaflet's micro-environment during physiological and pathological loading. This study's important biomechanical findings can be summarized as follows: (i) the atrialis layer of both selected leaflets (MVAL and TVAL) exhibited an apparent toe region and a significant mechanical compliance; (ii) the average peak and preconditioning stretches of the intact TVAL were bounded between those responses of the A/S and F/V layers in the circumferential direction; (iii) contrary to the aortic valve (AV)

leaflets, the MVAL fibrosa and ventricularis layers showed a nearly isotropic behavior. However, since no previous literature exists on the mechanical properties of the distinct fibrosa and ventricularis layers for the atrioventricular heart valve leaflets, this observed relationship will be further discussed in Section 4.2.

4.1.1. Extensibility of the atrialis/spongiosa layer—Histological analyses revealed the MVAL atrialis/spongiosa to be composed of 35.0% elastin and the TVAL atrialis/spongiosa to be of approximately 19.3% elastin (Tables 1 and 2). The elastin fibers, intricately coupled with collagen, allow biological tissues to extend beyond the free length of the collagen fibers alone. Based on our histological results, the atrialis elastin was determined to be present in two forms: (i) continuous, radially-oriented fibers and (ii) wisp-like strands in the circumferential direction. The extensibility of the atrialis/spongiosa therefore is likely a result of the radially-oriented elastin. However, collagen fiber arrangement limits the deformation of this layer in the circumferential direction, resulting in a material anisotropy similar to that observed in intact heart valve leaflets. Also, the TVAL-A/S contained nearly 15% more GAGs than the MVAL-A/S layer. The peak tissue stretch was 6.1% and 9.0% greater in the radial direction than in the circumferential direction for the MVAL-A/S and the TVAL-A/S, respectively (Table 3). Interestingly, this anisotropy is attributed to preconditioning (Table 1, Fig. 6a–d), whereas the mechanical stretch was shown to be similar in the circumferential and radial directions (Table 4, Fig. 7a, Fig. 9a).

While valvular layer-specific investigations are limited, the few studies conducted on the mitral valve and the aortic valve have reported similar morphological findings and tissue biomechanics. In a previous study [8], the ECM quantification yielded the following mass fractions: elastin: A/S-39.9%, F-8.8%, V-55.5%; collagen: A/S-21.7%, F-67.1%, V-30.9%; and GAGs: A/S-38.4%, F-24.1%, V-13.6%. These mass fractions are consistent with our histological findings (Table 2). Comparatively, the ventricularis of the aortic valve is anatomically analogous to the atrioventricular valve atrialis. This layer is analogous due to its relative geometry but defined conversely for its varied anatomical position. Studies on this aortic ventricularis have similarly found the thin, elastic layer to be extremely compliant [11,38]. Both earlier studies also referenced the contribution made by the exterior layers in reducing the radial stretches, particularly in the low-stress region.

4.1.2. Isotropy of the MVAL fibrosa and ventricularis—Extensive investigations of the intact MVAL have characterized the leaflet as nonlinear and anisotropic [10,20,22–26]. The orientation of the leaflet's abundant collagen network, concentrated in the fibrosa, runs parallel to the physiological loading direction to support cardiac loading. Consequently, it has been hypothesized that the dense fibrosa layer behaves most analogous to the intact leaflet under tensile testing. However, our results indicate that the separated fibrosa exhibits isotropic mechanical behaviors. Vesely and Noseworthy [38] described a similar phenomenon in the aortic valve fibrosa, attributing such nonconformity to collagen fiber elongation post-microdissection. Post-microdissection fibrillar elongation was further documented in Stella and Sacks [11], reporting that the fibrosa deformed 28.2% and 4.8% in the radial and circumferential directions, respectively. The collagen fiber elongation after the removal of the interlayer attachments may be attributed to the previous findings that the

fibrosa unfolds because the layer is naturally under a state of biaxial compression [11,38,40]. Another possible explanation for the observed isotropy of the fibrosa layer could be due to the loss of critical interactions between collagen fibers and the ground matrix. The ground matrix is responsible for regulating fiber recruitment, and without an interaction with the fibrosa insufficient fiber recruitment may result in the nearly isotropic response [38,40–42]. The biomechanical importance of fiber-orientation has been underscored in heart valve tissue mechanics as well as for other highly aligned collagenous tissues [43–46]. In this case, the flattening of these collagen fibers decreased the extent of mechanical deformation experienced during testing.

No previous studies have investigated the separated ventricularis. We were able to, *for the first time*, show that this layer comprises a similar percentage of the total MVAL leaflet thickness as the atrialis/spongiosa layer (30.4% and 34.5%, respectively). Additionally, the ventricularis constituent's percent composition demonstrates a larger collagen presence than that of the atrialis/spongiosa (49.9% and 34.8%, respectively) (Table 2), and the mechanical properties are starkly different (Fig. 8a–e). The ECM distribution, based on image quantification, is consistent with previous literature [8]. The isotropic response of the tissue and limited extensibility require additional study to clarify its functional role.

4.1.3. Comparisons of biaxial mechanical behaviors between the MVAL and TVAL—In both the MVAL and TVAL specimens, considerable preconditioning stretches were observed, which may be attributed to the release of the inherent pre-stress in the tissue collectively caused by (i) heart dissection from the porcine animal, (ii) leaflet dissection from the heart, (iii) the employed layer separation procedure, and (iv) tissue sectioning prior to mounting to the biaxial mechanical testing system. Similar preconditioning stretches for the aortic valve leaflet tissues were also observed in the previous studies by Stella and Sacks [11] and Billiar and Sacks [43]. The TVAL fibrosa/ventricularis layer displayed the greatest degree of anisotropy (AI = 1.12), whereas the MVAL fibrosa and ventricularis layers (AI = 1.01, 1.01) responded in the most isotropic fashion to the applied equibiaxial tension (Table 3, Fig. 5a, Fig. 8a). The toe regions of the stress-stretch curve for the combined F/V of the TVAL and the separated F and V of the MVAL were more linear than that of the atrialis/spongiosa layers. Both MVAL and TVAL atrialis/spongiosa layers displayed a distinct toe region as the transition from low to high stress occurred. This compliant mechanical response suggests that the layer microstructure plays a contributory role in managing the stress experienced by the intact leaflet during cardiac function.

4.1.4. Comparisons of the biaxial mechanical behavior of layers with the microstructural compositions—Comparing the individual mechanical response and the microstructure of each layer provides potential insight between the relationship of microstructure and mechanics. In the MVAL and TVAL, the atrialis/spongiosa layer showed the greatest extensibility of the separated layers, while also containing the lowest mass fraction of collagen (34.8% and 36.1%, respectively) (Tables 1 and 2, Fig. 5). This finding is expected, as collagen is the primary load-bearing constituent. Regarding the MVAL-V and MVAL-F layers, interestingly the ventricularis layer demonstrated lower extensibility than the fibrosa layer, despite having a lower collagen content (49.9% and 72.2%, respectively)

(Table 2, Fig. 8). However, the MVAL ventricularis layer did have a larger mass fraction of GAGs and elastin than the MVAL fibrosa layer, suggesting essential interactions exist between the three constituents that influence the mechanical response of the separated layers.

4.1.5. Thickness measurements—Variance in the intact specimen tissue thickness measurements, recorded prior to micro-dissection, emphasized anatomical discrepancies between different porcine animals (MVAL thickness range: 0.67–1.30 mm, TVAL thickness range: 0.55–0.90 mm). Such thickness variations underscore the necessity for patient-specific modeling capabilities. Additionally, we determined that there was a marked decrease in the sum of the average layer thicknesses in comparison to the average intact thickness measurements. The discrepancy was investigated using microscope images and ImageJ to precisely measure the thickness. Due to difficulties in accurately measuring biological soft tissue, the histological evaluation yielded minutely different thickness measurements, but none were fully able to account for the disparity. Therefore, we assumed that the difference was owed to micro-dissection. As previously discussed, the decrease in total thickness can be at least partially attributed to the rapid flattening of the fibrosa. Additionally, intact thickness measurements varied significantly across the leaflet, especially at chordae attachment points, which may have inflated the original thickness. Another potential source of change in leaflet geometry could be in the release of residual stresses/strains after layer separation. Finally, we hypothesized that ground substance and water enclosed within the intact tissue were released during microdissection, decreasing the tissue thickness, thus warranting future investigation.

4.1.6. Comparison to physiological loading conditions—Our mechanical testing procedure was developed such that it closely represents the maximum physiological loading of the tissue *in vivo.* In regard to the physiological stress, our procedure was developed based on previous literature [10,20,24] (cf. Section 2.3). As for the physiological strains, previous studies have found *ex vivo* stretch values for the TVSL to be 1.06 in the circumferential direction and 1.05 in the radial direction. Additionally, the MVAL stretch was quantified *in vitro* as 1.12 ± 0.04 for the circumferential direction and 1.39 ± 0.03 for the radial direction in our previous study [18]. Comparing to the mechanical stretch values from equibiaxial loading ($T_{circ,max}$:$T_{rad,max}$ = 1:1), our results are in line with the previously reported values (MVAL-A/S: 1.12 ±0.01, F: 1.14 ±0.01, V: 1.12 ±0.01; TVAL-A/S: 1.10 ±0.01, F/V: 1.11 ±0.02).

4.2. Study limitations and future work

Several limitations arise from the methodology described in this study. First, the micro-dissection procedure used to obtain the leaflet layers could potentially damage the tissue and it also results in relatively small effective testing size (~3.5 mm) the compared to previous biaxial mechanical studies of heart valve leaflet tissues (6.5–10 mm) [10,20,47]. Second, in previous studies it has been shown that the mechanical behavior of heart valve leaflets is loading-rate dependent [48,49]; however, due to the limitations of the CellScale BioTester system, in the current study it was not possible to investigate such a loading-rate dependency as close to the *in vivo* physiological function of the atrioventricular heart valves. Third, tine-

based BioRakes mounting mechanism limits the potential for shear that may be present during physiological function. Negligible shear-induced effect could be achieved by properly aligning the tissue's circumferential and radial directions with the biaxial testing system's X- and Y-axes. Fourth, the thickness measurements obtained via the dial caliper method may not be as accurate as those by other non-contact measurement techniques, such as optical coherence tomography (OCT); nevertheless, in our previous study we have shown that the dial caliper method agrees reasonably with thickness measurements obtained via histological methods (cf. Table 6 & Figure 10 in Jett *et al.,* 2018 [10]). Fifth, our biaxial testing protocol considered five independent loading protocols, while a previous study has shown that seven protocols may resolve a more comprehensive range of the valve's mechanical responses (i.e., $T_{circ,max}$:$T_{rad,max}$ = 1:1, 0.5:1, 1:0.5, 0.333:1, 1:0.333, 0:1, and 1:0) [50]. Sixth, although our calculation of the anisotropy index utilized the stretch values associated with different stresses for each layer, these results were obtained based on the applied membrane tension values, which were the same across all specimens of each valve. Finally, the present work and a recent study by our group [27] have shown variations in the biaxial mechanical responses of the atrioventricular heart valve leaflet tissues spatially and through tissue layers. Such intricate regionally-varied microstructure, which was not adequately considered in the previous literature of heart valve biomechanical computations, necessitates the future refinement of valve-specific computational models for more accurately predicting diseased or surgically-intervened condition, where tissue heterogeneity plays an essential role in the heart valve function. Another minor limitation includes the relatively small sample size (n = 6).

The fundamental extension of this study is the development of a high-fidelity, informed computational model based on the layer stress-stretch behavior obtained in this study. Additionally, the characterization of the MVAL-V and TVAL layers, *for the first time,* provides a valuable starting point for explaining leaflet structure-function relationship. The data would be especially useful in the development of constitutive models for the AHVs, as the layer-specific behaviors can be used to better inform the bulk-tissue level behaviors. However, even with these data, the contribution of the ventricularis and spongiosa remain largely unexplained. Based on the layer-specific properties of the atrialis/spongiosa and the fibrosa, further study of the spongiosa and ventricularis are likely to provide valuable insight into the function of the layers' respective morphologies. Moreover, collagen fiber microstructural architecture, including fiber orientation and fiber dispersion, has found to be essential for developing constitutive models of soft biological tissues incorporating both the mechanical and structural features [51]. Future work is warranted to quantify the fiber dispersion in the atrioventricular valve leaflets as included in biomechanical computational modeling. Another future extension of this work would be the testing of the individual AHV leaflet layers for those tissues not tested in this work (MVPL, TVPL, and TVSL).

From a clinical standpoint, further understanding of the leaflet structure-function relationship is critical. For example, mitral valve repair is associated with better cardiac function, lower mortality and longer survival when compared to valve replacement for degenerative mitral regurgitation [52–54]. One has to wonder what functional advantages keeping the native valve in place versus replacing it with a prosthetic valve provides. Expanding our insight into the leaflet structure-function relationship will undoubtedly help

to guide novel valve repair techniques as well as the development of new, more physiologic prosthetic valve replacements.

4.3. Conclusion

In this novel study, we have quantified the microstructural composition and biaxial mechanical properties of the mitral and tricuspid valve anterior leaflet layers. Mechanical functions of the leaflet constituents have been examined in light of the percent composition of the microstructure of each layer. The elastin-rich atrialis/spongiosa layer has been shown to be the most compliant and anisotropic examined layer. Accordingly, the fibrosa and ventricularis layers have been shown to have a smaller toe region and a nearly isotropic behavior. When comparing mechanical data obtained in this study to that of a previous study by our group, we have determined that the material behavior of the intact tissue did not match any specific layer. Our results thus indicate that the previously adopted homogenous leaflet may be an oversimplification of the complex leaflet anatomy. As part of our future extensions, we plan to incorporate biomechanical findings from this study into our computational model to best simulate native valve function.

Supplementary Material

Refer to Web version on PubMed Central for supplementary material.

Acknowledgments

Support from the American Heart Association Scientist Development Grant (SDG) Award (16SDG27760143) is gratefully acknowledged. We also acknowledge Dr. Kar-Ming Fung from the Department of Pathology at the OU Health Sciences Center (OUHSC) for his help in the histological study. CHL was in part supported by the institutional start-up funds from the School of Aerospace and Mechanical Engineering (AME) and the research funding through the Faculty Investment Program from the Research Council and the IBEST-OUHSC Interdisciplinary Funding at the University of Oklahoma (OU). KEK and CJR were supported by the Mentored Research Fellowship from the Office of Undergraduate Research and the Undergraduate Research Opportunities Program from the Honors College at OU.

Nomenclature

AHV	Atrioventricular heart valve
AV	Aortic valve
AL	Anterior leaflet
MV	Mitral valve
MVAL	Mitral valve anterior leaflet
MVPL	Mitral valve posterior leaflet
PL	Posterior leaflet
SL	Septal leaflet
TV	Tricuspid valve

TVAL	Tricuspid valve anterior leaflet
TVPL	Tricuspid valve posterior leaflet
TVSL	Tricuspid valve septal leaflet
A	Atrialis layer
A/S	Combined atrialis and spongiosa layer
ECM	Extracellular matrix
F	Fibrosa layer
GAG	Glycosaminoglycan
PG	Proteoglycan
S	Spongiosa
V	Ventricularis layer
F/V	Combined fibrosa and ventricularis layer
VIC	Valve interstitial cell
AI	Anisotropy index
C	Right Cauchy-Green tensor
F	Deformation gradient tensor
$\boldsymbol{f_{circ}}$	Force applied to the tissue specimen in the circumferential direction
$\boldsymbol{f_{rad}}$	Force applied to the tissue specimen in the radial direction
$\boldsymbol{J}$	Determinant of **F** (volume ratio)
$\boldsymbol{L}$	Effective specimen size, i.e., tine-to-tine distance
λ_{circ}^{0-peak}	Peak tissue stretch in the circumferential direction
λ_{circ}^{0-1}	Preconditioning stretch in the circumferential direction
λ_{circ}^{1-peak}	Mechanical stretch in the circumferential direction
λ_{rad}^{0-peak}	Peak tissue stretch in the radial direction
λ_{rad}^{0-1}	Preconditioning stretch in the radial direction
λ_{rad}^{1-peak}	Mechanical stretch in the radial direction

Ω_0	Tissue-mounting configuration prior to the preconditioning step
Ω_1	Post-preconditioning configuration
P	First Piola-Kirchhoff stress tensor
S	Second Piola-Kirchhoff stress tensor
σ	Cauchy stress tensor
t	Thickness of the tissue specimen
T_{circ}	Membrane tension applied in the circumferential direction
$T_{circ,max}$	Peak membrane tension applied in the circumferential direction
T_{rad}	Membrane tension applied in the radial direction
$T_{rad,max}$	Peak membrane tension applied in the radial direction
circ	Tissue’s circumferential direction
DIC	Digital image correlation
MRI	Magnetic resonance imaging
PBS	Phosphate-buffered saline
rad	Tissue’s radial direction
SEM	Standard error of the mean

References

[1]. Nkomo VT, Gardin JM, Skelton TN, Gottdiener JS, Scott CG, Enriquez-Sarano M, Burden of valvular heart diseases: a population-based study, Lancet 368 (9540)(2006) 1005–1011. [PubMed: 16980116]

[2]. Flameng W, Herijgers P, Bogaerts K, Recurrence of mitral valve regurgitation after mitral valve repair in degenerative valve disease, Circulation 107 (12) (2003)1609–1613. [PubMed: 12668494]

[3]. Rodés-Cabau J, Taramasso M, O’Gara PT, Diagnosis and treatment of tricuspid valve disease: current and future perspectives, Lancet 388 (10058) (2016) 2431–2442. [PubMed: 27048553]

[4]. Dreyfus GD, Corbi PJ, Chan KMJ, Bahrami T, Secondary tricuspid regurgitation or dilatation: Which should be the criteria for surgical repair?, Ann Thorac. Surg. 79 (1) (2005) 127–132. [PubMed: 15620928]

[5]. Shiran A, Sagie A, Tricuspid regurgitation in mitral valve disease: incidence, prognostic implications, mechanism, and management, J. Am. Coll. Cardiol. 53 (5) (2009) 401–408. [PubMed: 19179197]

[6]. Zeybek R, Ay Y, Ay NK, Tekumit H, Aydin C, Tricuspid valve repair: an old disease, a modern experience, Am. J. Cardiol. 121 (8) (2018) e136–e137.

[7]. Stephens EH, Borger MA, “Forgotten” valve or “enigmatic” valve? Further insights into the tricuspid valve in patients undergoing mitral valve surgery, J. Thorac. Cardiovasc. Surg. 148 (5) (2014) 1962–1964. [PubMed: 25444187]

[8]. Lee C-H, Carruthers CA, Ayoub S, Gorman RC, Gorman III JH, Sacks MS, Quantification and simulation of layer-specific mitral valve interstitial cells deformation under physiological loading, J. Theor. Biol. 373 (2015) 26–39. [PubMed: 25791285]

[9]. Misfeld M, Sievers HH, Heart valve macro-and microstructure, Philos. Trans. R. Soc. London B Biol. Sci. 362 (2007) 1421–1436. [PubMed: 17581807]

[10]. Jett SV, Laurence DW, Kunkel RP, Babu AR, Kramer KE, Baumwart R, Towner RA, Wu Y, Lee C-H, An investigation of the anisotropic mechanical properties and anatomical structure of porcine atrioventricular heart valves, J. Mech. Behav. Biomed. Mater. 87 (2018) 155–171. [PubMed: 30071486]

[11]. Stella JA, Sacks MS, On the biaxial mechanical properties of the layers of the aortic valve leaflet, J. Biomech. Eng. 129 (5) (2007) 757–766. [PubMed: 17887902]

[12]. Sacks MS, Yoganathan AP, Heart valve function: a biomechanical perspective, Philos. Trans. R. Soc. London B: Biol. Sci. 362 (1484) (2007) 1369–1391. [PubMed: 17588873]

[13]. McCarthy KP, Ring L, Rana BS, Anatomy of the mitral valve: understanding the mitral valve complex in mitral regurgitation, Eur. J. Echocardiogr. 11 (10) (2010) i3–i9. [PubMed: 21078837]

[14]. Sun W, Martin C, Pham T, Computational modeling of cardiac valve function and intervention, Annu. Rev. Biomed. Eng. 16 (2014) 53–76. [PubMed: 24819475]

[15]. Padala M, Patient-specific computational biomechanical modeling to guide mitral valve repair strategy: practicality and value?, J Thorac. Cardiovasc. Surg. 155 (2) (2018) 606–607. [PubMed: 29415388]

[16]. Stevanella M, Maffessanti F, Conti CA, Votta E, Arnoldi A, Lombardi M, Parodi O, Caiani EG, Redaelli A, Mitral valve patient-specific finite element modeling from cardiac MRI: application to an annuloplasty procedure, Cardiovasc. Eng. Technol. 2 (2) (2011) 66–76.

[17]. Lee LC, Genet M, Dang AB, Ge L,Guccione JM, Ratcliffe MB, Applications of computational modeling in cardiac surgery, J. Card. Surg. 29 (3) (2014) 293–302. [PubMed: 24708036]

[18]. Lee C-H, Rabbah J-P, Yoganathan AP, Gorman RC, Gorman III JH, Sacks MS, On the effects of leaflet microstructure and constitutive model on the closing behavior of the mitral valve, Biomech. Model. Mechanobiol. 14 (6) (2015) 1281–1302. [PubMed: 25947879]

[19]. Lee C-H, Zhang W, Feaver K, Gorman RC, Gorman JH 3rd, Sacks MS, On the in vivo function of the mitral heart valve leaflet: Insights into tissue-interstitial cell biomechanical coupling, Biomech. Model. Mechanobiol. 16 (5) (2017) 1613–1632. [PubMed: 28429161]

[20]. Khoiy KA, Amini R, On the biaxial mechanical response of porcine tricuspid valve leaflets, J. Biomech. Eng. 138 (10) (2016) 104504–104504–6.

[21]. Jett SV, Laurence DW, Kunkel RP, Babu AR, Kramer KE, Baumwart R, Towner RA, Wu Y, Lee C-H, Biaxial mechanical data of porcine atrioventricular valve leaflets, Data in Brief 21 (2018) 358–363. [PubMed: 30364794]

[22]. Grashow JS, Sacks MS, Liao J, Yoganathan AP, Planar biaxial creep and stress relaxation of the mitral valve anterior leaflet, Ann. Biomed. Eng. 34 (10) (2006)1509–1518. [PubMed: 17016761]

[23]. May-Newman K, Yin FC, Biaxial mechanical behavior of excised porcine mitral valve leaflets, Am. J. Physiol. Heart Circ. Physiol. 269 (4) (1995) H1319–H1327.

[24]. Pierlot CM, Moeller AD, Lee JM, Wells SM, Biaxial creep resistance and structural remodeling of the aortic and mitral valves in pregnancy, Ann. Biomed. Eng. 43 (8) (2015) 1772–1785. [PubMed: 25564325]

[25]. Pham T, Sulejmani F, Shin E, Wang D, Sun W, Quantification and comparison of the mechanical properties of four human cardiac valves, Acta Biomater. 54 (2017) 345–355. [PubMed: 28336153]

[26]. Pham T, Sun W, Material properties of aged human mitral valve leaflets, J. Biomed. Mater. Res. A 102 (8) (2014) 2692–2703. [PubMed: 24039052]

[27]. Laurence DW, Ross CJ, Jett SV, Johns CH, Echols AL, Baumwart R, Towner RA, Liao J, Bajona P, Wu Y, Lee C-H, An investigation of regional variations in the biaxial mechanical properties and stress relaxation behaviors of porcine atrioventricular heart valve leaflets, J. Biomech. 83 (2019) 16–27. [PubMed: 30497683]

[28]. Rego BV, Sacks MS, A functionally graded material model for the transmural stress distribution of the aortic valve leaflet, J. Biomech. 54 (2017) 88–95. [PubMed: 28256242]

[29]. Arzani A, Mofrad MRK, A strain-based finite element model for calcification progression in aortic valves, J. Biomech. 65 (2017) 216–220. [PubMed: 29100595]

[30]. Prot V, Skallerud B, Nonlinear solid finite element analysis of mitral valves with heterogeneous leaflet layers, Comput. Mech. 43 (3) (2009) 353–368.

[31]. Prot V, Skallerud B, Holzapfel GA, Transversely isotropic membrane shells with application to mitral valve mechanics. Constitutive modelling and finite element implementation, Int. J. Numer. Meth. Eng. 71 (8) (2007) 987–1008.

[32]. Woo SL-Y, Orlando CA, Camp JF, Akeson WH, Effects of postmortem storage by freezing on ligament tensile behavior, J. Biomech. 19 (5) (1986) 399–404. [PubMed: 3733765]

[33]. Bernacca GM, O'Connor B, Williams DF, Wheatley DJ, Hydrodynamic function of polyurethane prosthetic heart valves: influences of Young's modulus and leaflet thickness, Biomaterials 23 (1) (2002) 45–50. [PubMed: 11762853]

[34]. Vesely I, The role of elastin in aortic valve mechanics, J. Biomech. 31 (2) (1998) 115–123. [PubMed: 9593204]

[35]. Huang H-YS, Liao J, Sacks MS, In-situ deformation of the aortic valve interstitial cell nucleus under diastolic loading, J. Biomech. Eng. 129 (6) (2007) 880–889. [PubMed: 18067392]

[36]. Flanagan TC, Black A, O'Brien M, Smith TJ, Pandit AS, Reference models for mitral valve tissue engineering based on valve cell phenotype and extracellular matrix analysis, Cells Tissues Organs 183 (1) (2006) 12–23. [PubMed: 16974091]

[37]. Ruifrok AC, Johnston DA, Quantification of histochemical staining by color deconvolution, Anal. Quant. Cytol. Histol. 23 (4) (2001) 291–299. [PubMed: 11531144]

[38]. Vesely I, Noseworthy R, Micromechanics of the fibrosa and the ventricularis in aortic valve leaflets, J. Biomech. 25 (1) (1992) 101–113. [PubMed: 1733978]

[39]. Kunzelman KS, Cochran RP, Murphree SS, Ring WS, Verrier ED, Eberhart RC, Differential collagen distribution in the mitral valve and its influence on biomechanical behaviour, J. Heart Valve Dis. 2 (2) (1993) 236–244. [PubMed: 8261162]

[40]. Vesely I, Lozon A, Natural preload of aortic valve leaflet components during glutaraldehyde fixation: Effects on tissue mechanics, J. Biomech. 26 (2) (1993) 121–131. [PubMed: 8429055]

[41]. Bellini C, Ferruzzi J, Roccabianca S, Di Martino ES, Humphrey JD, A microstructurally motivated model of arterial wall mechanics with mechanobiological implications, Ann. Biomed. Eng. 42 (3) (2014) 488–502. [PubMed: 24197802]

[42]. Dingemans KP, Teeling P, Lagendijk JH, Becker AE, Extracellular matrix of the human aortic media: an ultrastructural histochemical and immunohistochemical study of the adult aortic media, Anat. Rec.: Off. Publ. Am. Assoc. Anatomists 258 (1) (2000) 1–14.

[43]. Billiar KL, Sacks MS, Biaxial mechanical properties of the natural and glutaraldehyde treated aortic valve cusp-Part I: experimental results, J. Biomech. Eng. 122 (1) (2000) 23–30. [PubMed: 10790826]

[44]. De Hart J, Peters GWM, Schreurs PJG, Baaijens FPT, Collagen fibers reduce stresses and stabilize motion of aortic valve leaflets during systole, J. Biomech. 37 (3) (2004) 303–311. [PubMed: 14757449]

[45]. Alavi SH, Sinha A, Steward E, Milliken JC, Kheradvar A, Load-dependent extracellular matrix organization in atrioventricular heart valves: differences and similarities, Am. J. Physiol. Heart Circ. Physiol. 309 (2) (2015) H276–H284. [PubMed: 26001411]

[46]. Niestrawska JA, Viertler C, Regitnig P, Cohnert TU, Sommer G, Holzapfel GA, Microstructure and mechanics of healthy and aneurysmatic abdominal aortas: experimental analysis and modelling, J. R. Soc. Interface 13 (124) (2016) 20160620.

[47]. Grashow JS, Yoganathan AP, Sacks MS, Biaixal stress-stretch behavior of the mitral valve anterior leaflet at physiologic strain rates, Ann. Biomed. Eng. 34 (2) (2006) 315–325. [PubMed: 16450193]

[48]. Anssari-Benam A, Tseng Y-T, Bucchi A, A transverse isotropic constitutive model for the aortic valve tissue incorporating rate-dependency and fibre dispersion: application to biaxial deformation, J. Mech. Behav. Biomed. Mater. 85 (2018) 80–93. [PubMed: 29859418]

[49]. Anssari-Benam A, Screen HRC, Bucchi A, Insights into the micromechanics of stress-relaxation and creep behaviours in the aortic valve, J. Mech. Behav. Biomed. Mater. 93 (2019) 230–245. [PubMed: 30844614]

[50]. Sacks MS, Biaxial mechanical evaluation of planar biological materials, J. Elast. 61 (1) (2000) 199.

[51]. Holzapfel GA, Niestrawska JA, Ogden RW, Reinisch AJ, Schriefl AJ, Modelling non-symmetric collagen fibre dispersion in arterial walls, J. R. Soc. Interface 12 (106) (2015) 20150188.

[52]. Yacoub M, Halim M, Radley-Smith R, McKay R, Nijveld A, Towers M, Surgical treatment of mitral regurgitation caused by floppy valves: repair versus replacement, Circulation 64 (2 Part 2) (1981). II210–6. [PubMed: 7249325]

[53]. Lazam S, Vanoverschelde J-L, Tribouilloy C, Grigioni F, Suri RM, Avierinos J-F, de Meester C, Barbieri A, Rusinaru D, Russo A, Pasquet A, Michelena HI, Huebner M, Maalouf J, Clavel MA, Szymanski C, Enriquez-Sarano M, MIDA (Mitral Regurgitation International Database) Investigators, Twenty-year outcome after mitral repair versus replacement for severe degenerative mitral regurgitation: analysis of a large, prospective, multicenter, international registry, Circulation 135 (5) (2017) 410–422. [PubMed: 27899396]

[54]. Ren J-F, Aksut S, Lighty GW Jr, Vigilante GJ, Sink JD, Segal BL, Hargrove III WC, Mitral valve repair is superior to valve replacement for the early preservation of cardiac function: Relation of ventricular geometry to function, Am. Heart J. 131 (5) (1996) 974–981. [PubMed: 8615319]

[55]. Sacks MS, A method for planar biaxial mechanical testing that includes in-plane shear, J. Biomech. Eng. 121 (5) (1999) 551–555. [PubMed: 10529924]

Health Research Alliance Author Manuscript

Statement of Significance

This study, which is *the first of its kind* for atrioventricular heart valve (AHV) leaflet tissue layers, rendered a mechanical characterization of the biaxial mechanical properties and distributions of extracellular matrix components (collagen, elastin, and glycosaminoglycans) of the mitral and tricuspid valve anterior leaflet layers. The novel findings from the present study emphasize the biomechanical variances throughout the thickness of AHV leaflets, and our results indicate that the previously-adopted homogenous leaflet in the AHV biomechanical modeling may be an oversimplification of the complex leaflet anatomy. Such improvement in the understanding of valvular morphology and tissue mechanics is crucial to future refinement of AHV computational models, serving as a patient-specific diagnostic and surgical tool, at the preoperative stage, for treating valvular heart diseases.

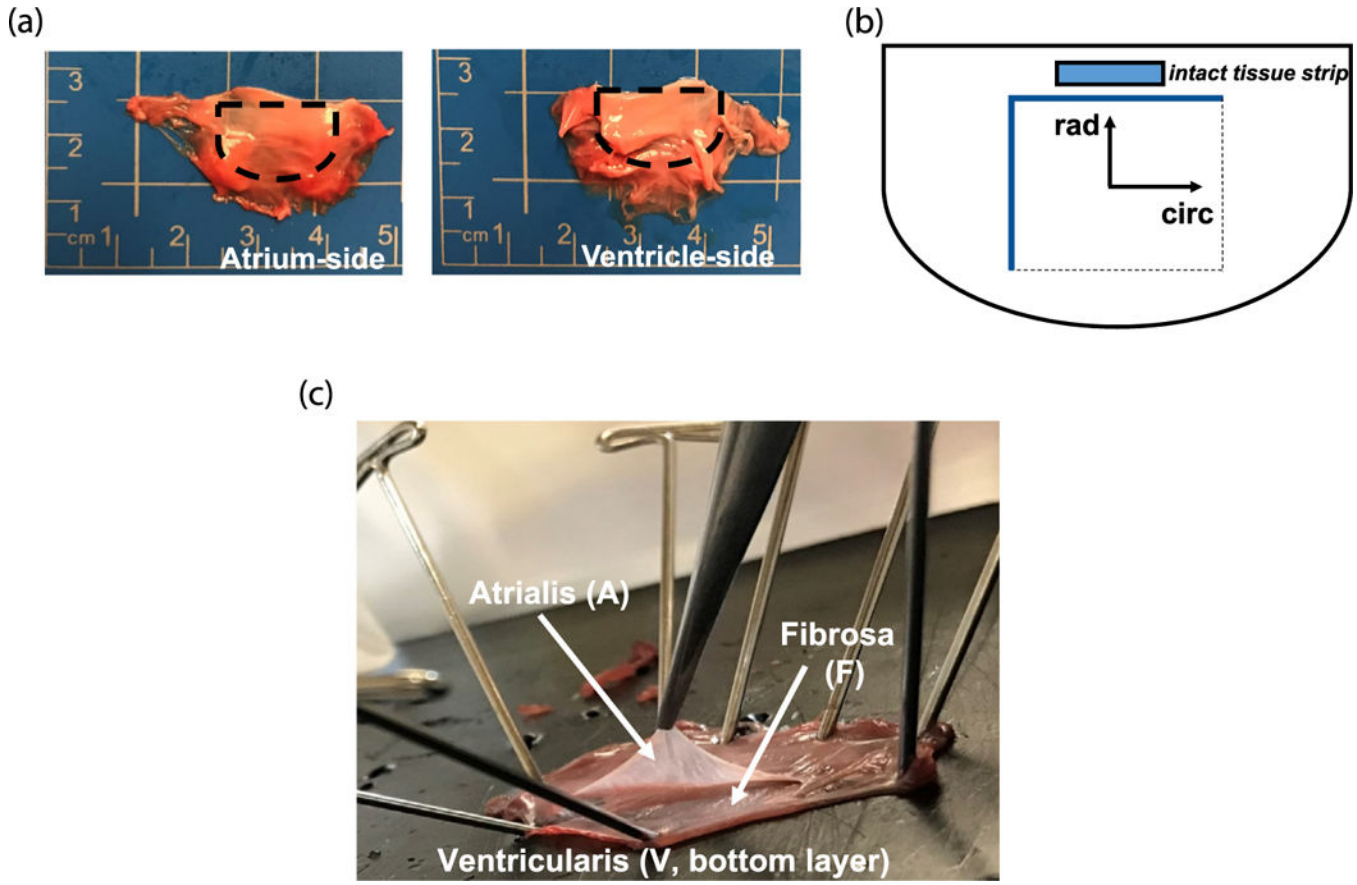

Fig. 1.

(a) Photos of a representative porcine mitral valve anterior leaflet tissue from both the atrial and ventricular sides of view. (b) Schematic of the clear zone of the MVAL or TVAL for performing the micro-dissection procedure. An intact tissue strip close to the valve annulus was used for thickness measurement and histologic quantification. (*circ*: circumferential direction, *rad*: radiation direction). (c) Micro-dissection process for a MVAL tissue, showing the atrialis layer first separated from the remaining tissue. 9/16″ head T-pins were used to fasten the tissue on a wax tray.

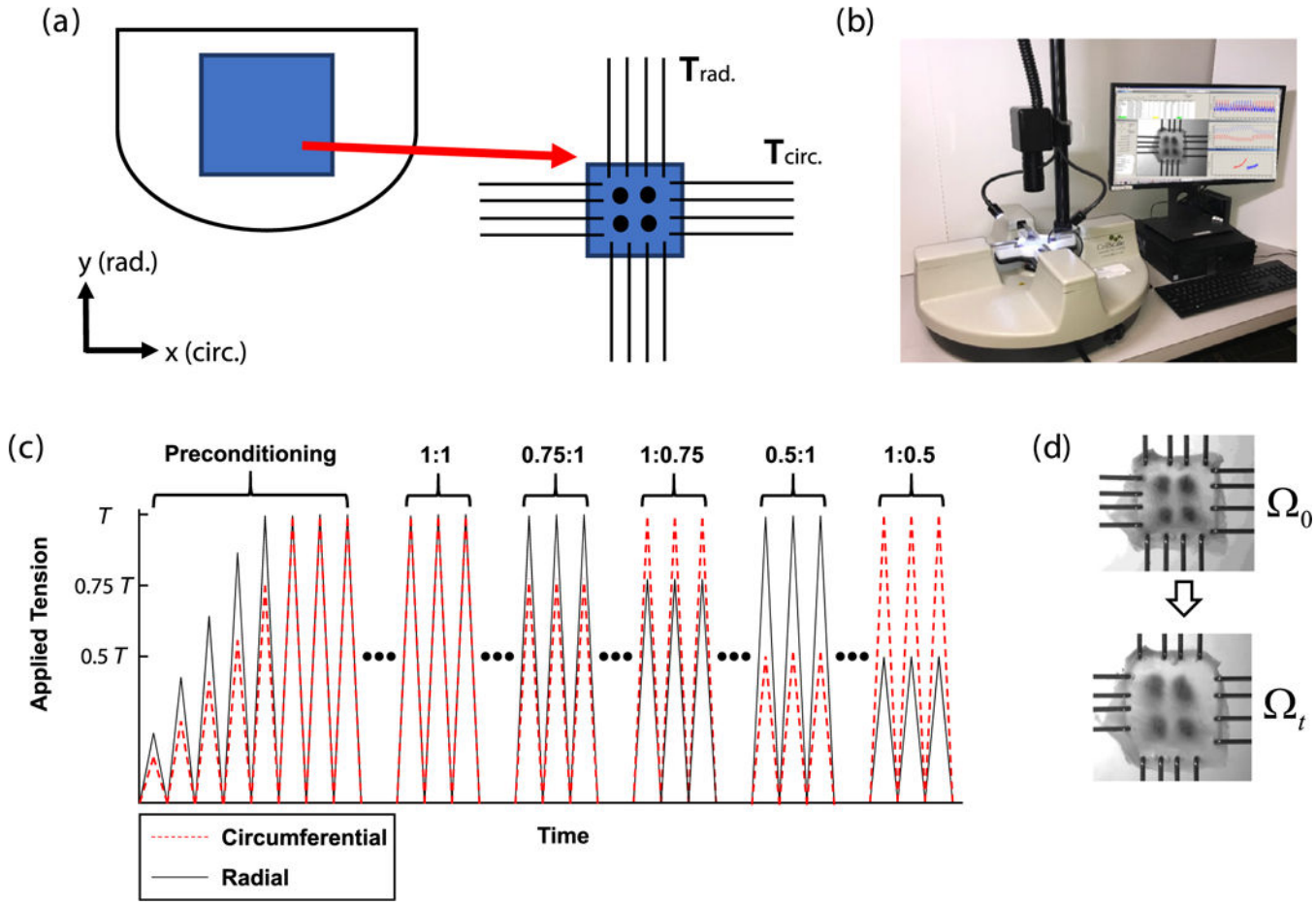

Fig. 2.

(a) Schematic of separated MVAL or TVAL layer tissue for biaxial mechanical testing with applied membrane tensions, T_{circ} and T_{rad}, along the *x*-(*circ.*) and *y*-(*rad.*) directions, respectively. (b) Commercial BioTester used in this study. (c) Schematic of the force-controlled biaxial mechanical testing protocols with 5 loading ratios ($T_{circ,max}$: $T_{rad,max}$ = 1:1, 0.75:1,1:0.75, 0.5:1, and 1:0.5). (d) Reference/undeformed configuration Ω_0 and deformed configuration Ω_t, showing the movement of four fiducial markers in accordance with tissue deformation. The marker positions were tracked by the DIC technique and the tracked marker coordinates were then used in the tissue's stretch calculations [10,43,50,55].

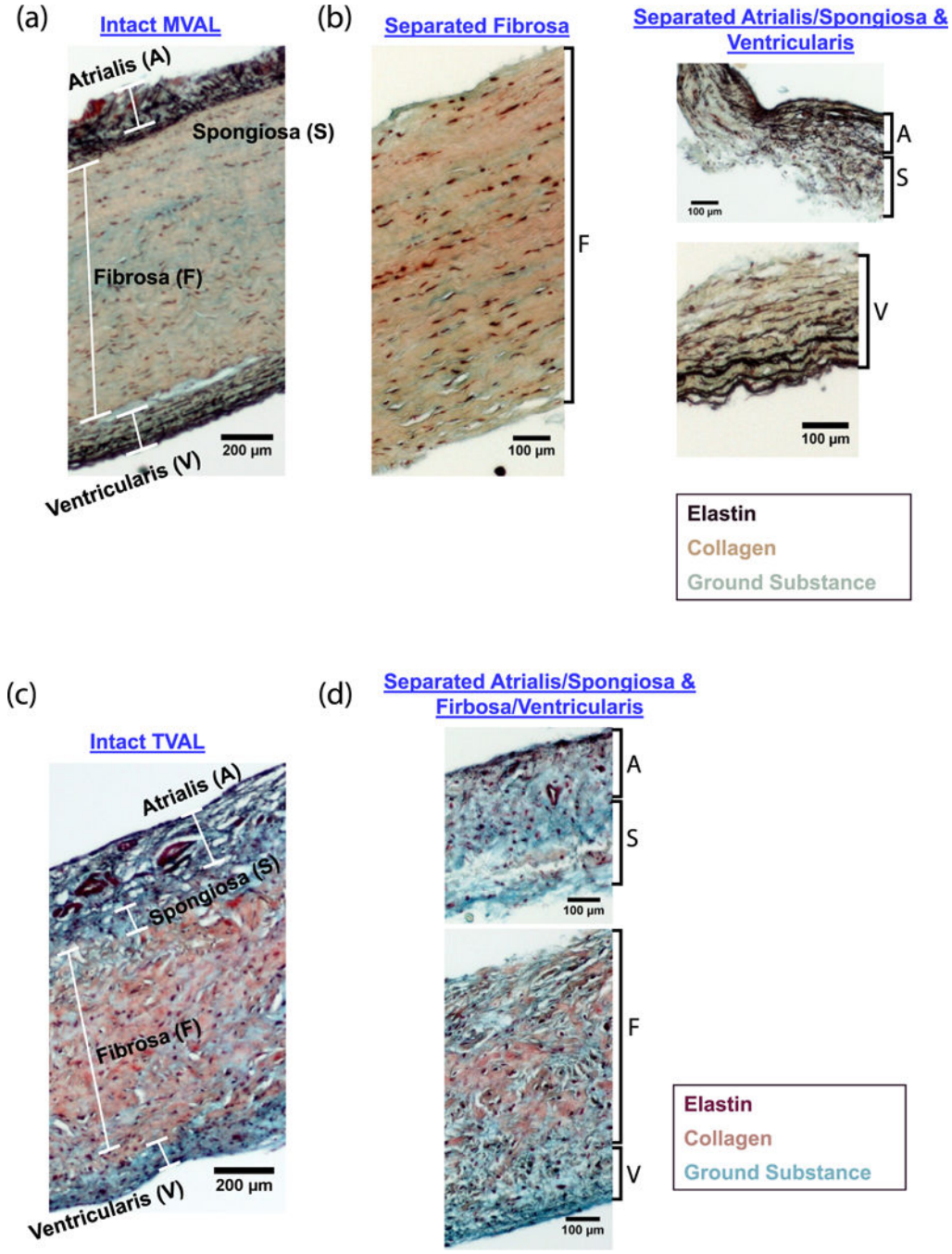

Fig. 3.

Histological images under Movat's pentachrome stain, confirming the successful separations of the tissue layers using the micro-dissection method: (a) intact MVAL tissue with four morphologically distinct layers (atrialis: A, spongiosa: S, fibrosa: F, and ventricularis: V), (b) separated fibrosa layer (F), combined atrialis/spongiosa (A/S), and ventricularis (V), (c) intact TVAL tissue, and (d) separated combined atrialis/spongiosa (A/S) layer and combined fibrosa/ventricularis (F/V) layer.

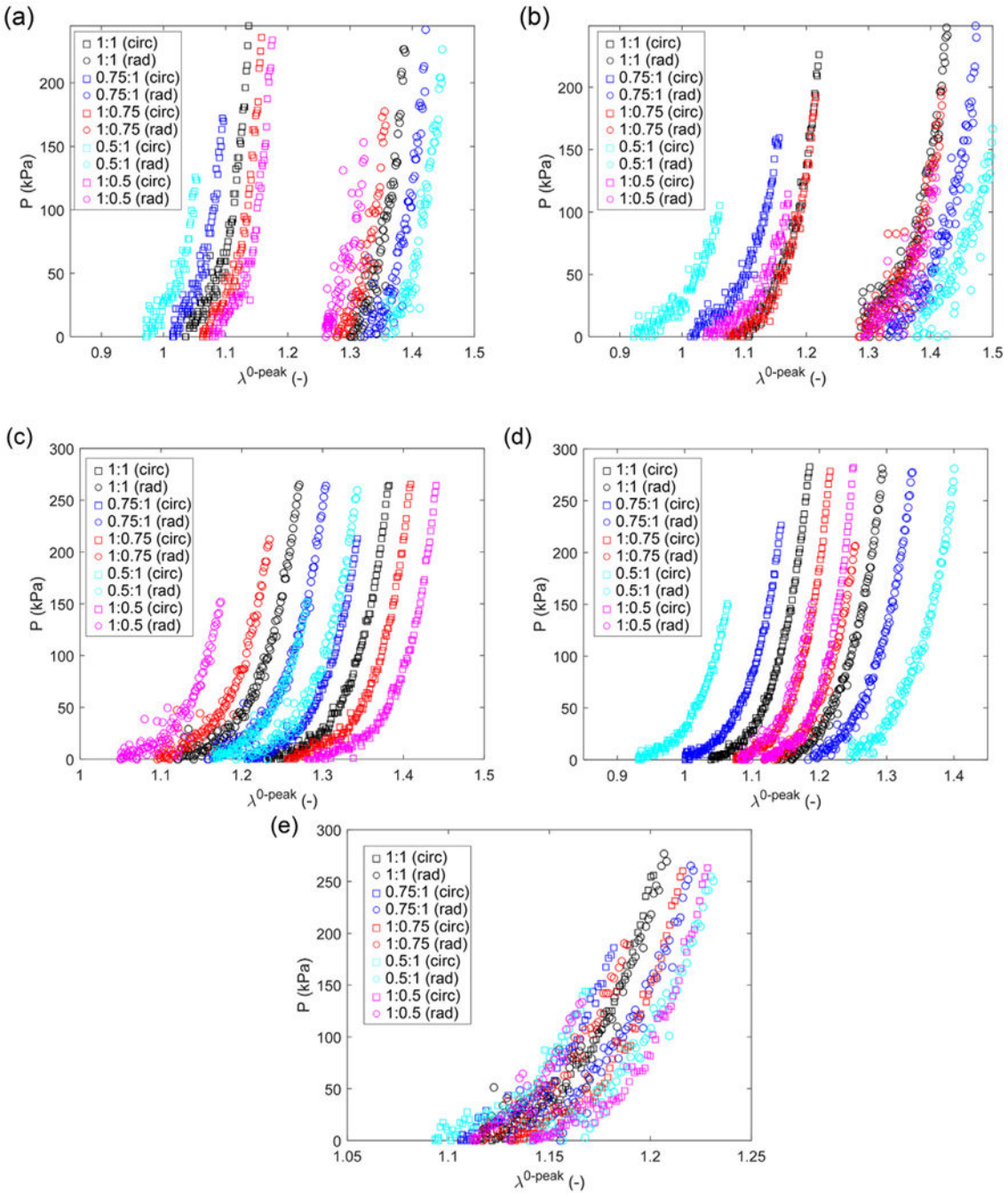

Fig. 4.

Representative biaxial mechanical testing results (first Piola-Kirchhoff stress versus peak tissue stretch): (a) TVAL-A/S, (b) TVAL-F/V, (c) MVAL-A, (d) MVAL-F, and (e) MVAL-V.

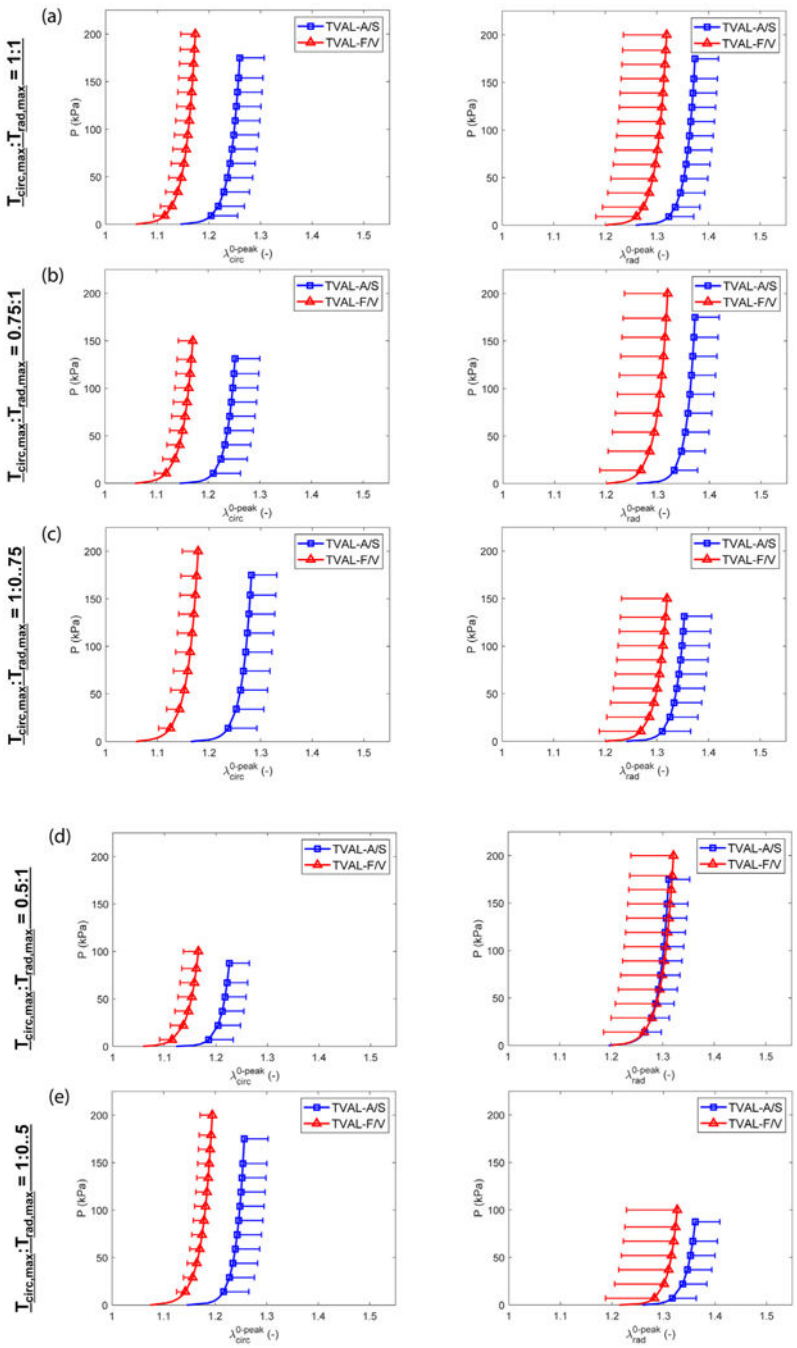

Fig. 5.

Mean ± SEM of the biaxial mechanical testing results (first Piola-Kirchhoff stress versus peak tissue stretch) of TVAL layer tissues (n = 6) under five force-controlled loading protocols: $T_{circ,max}$:$T_{rad,max}$ = (a) 1:1. (b) 0.75:1, (c) 1:0.75, (d) 0.5:1, and (e) 1:0.5.

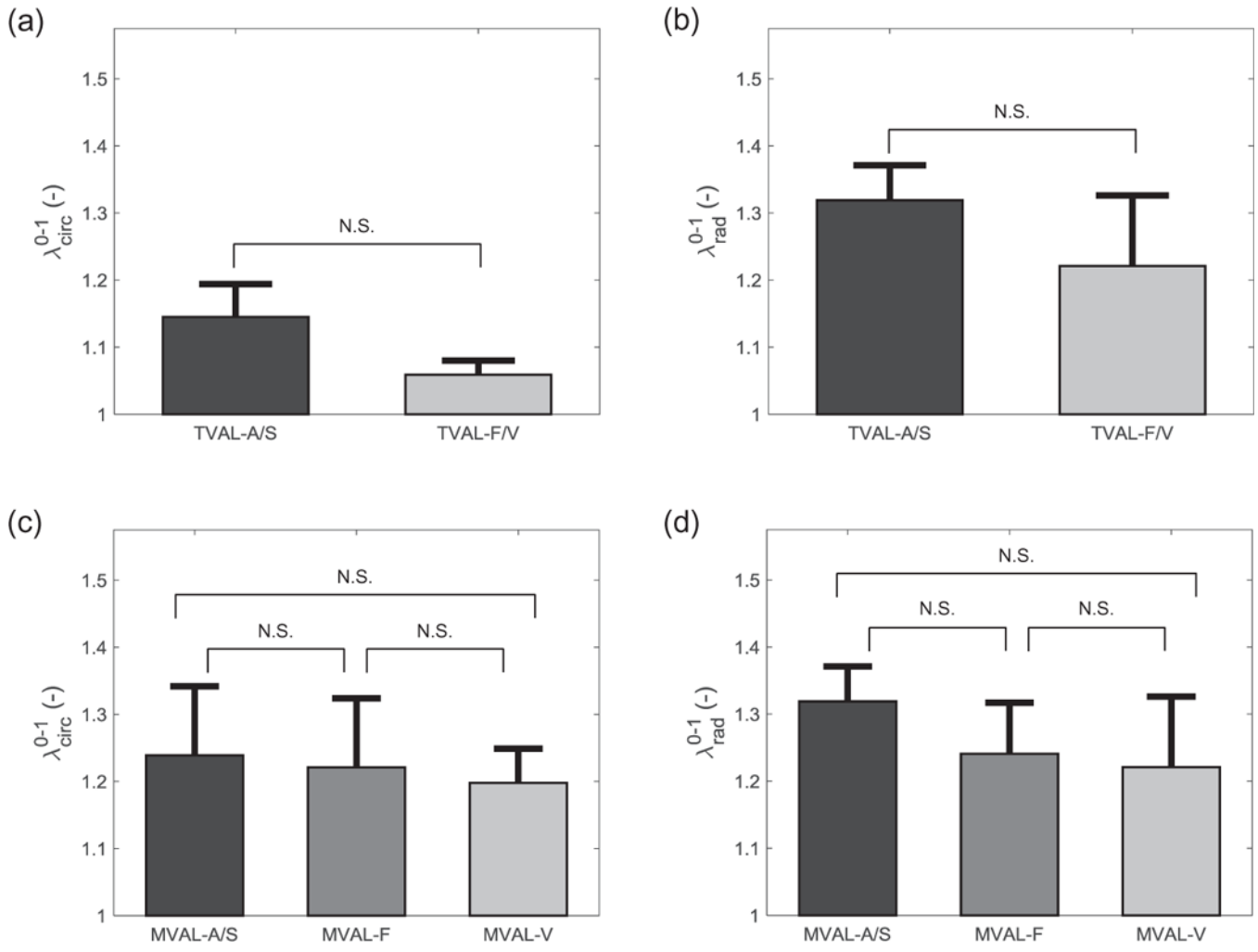

Fig. 6.

Comparisons of layer-specific preconditioning stretches of TVAL layers: (a) circumferential direction, (b) radial direction, and MVAL layers: (c) circumferential direction, (d) radial direction. (N.S.) denotes no statistically significant differences between the layers ($p > 0.1$).

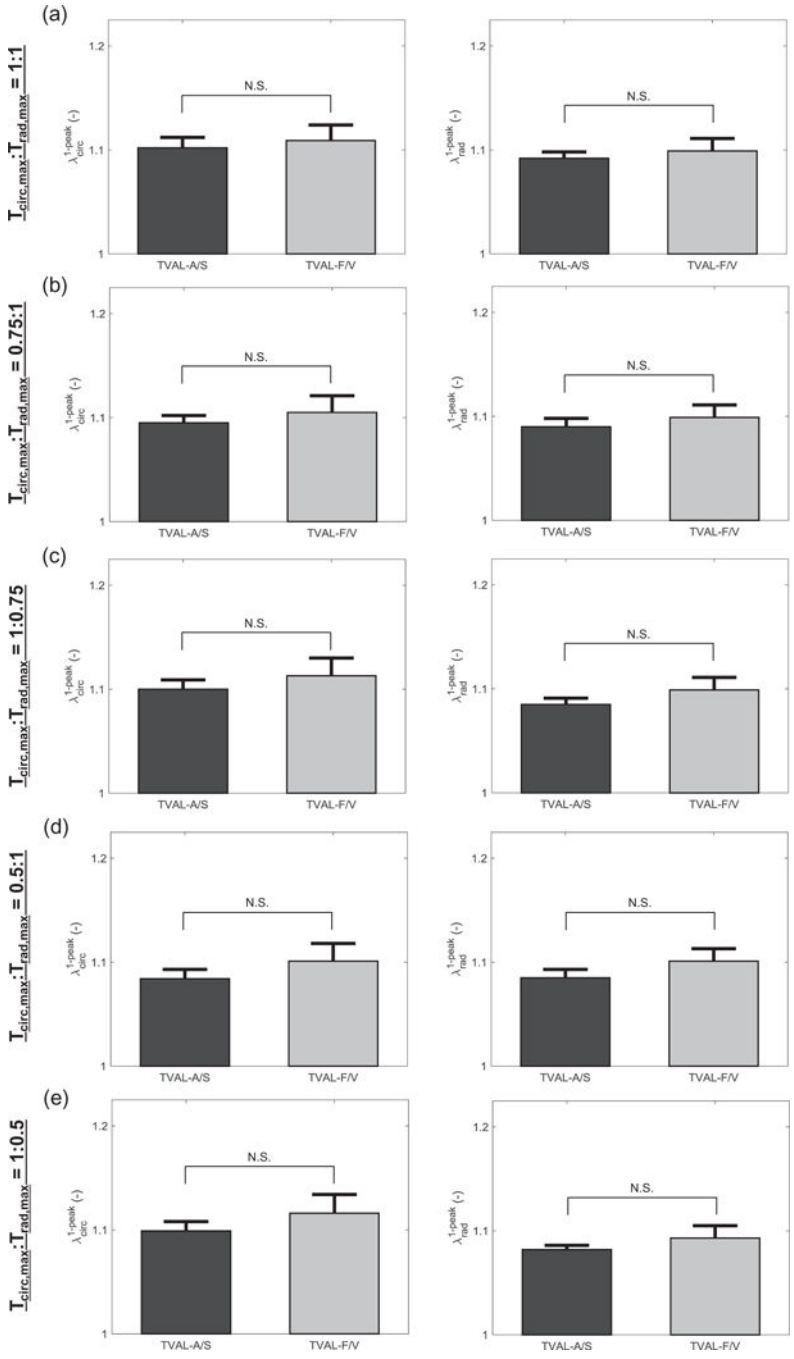

Fig. 7.

Comparisons of TVAL layer-specific mechanical stretches under five force-controlled loading protocols: $T_{circ,max}$:$T_{rad,max}$ = (a) 1:1, (b) 0.75:1, (c) 1:0.75, (d) 0.5:1, and (e) 1:0.5. (N.S.) denotes no statistically significant differences between the layers ($p > 0.1$).

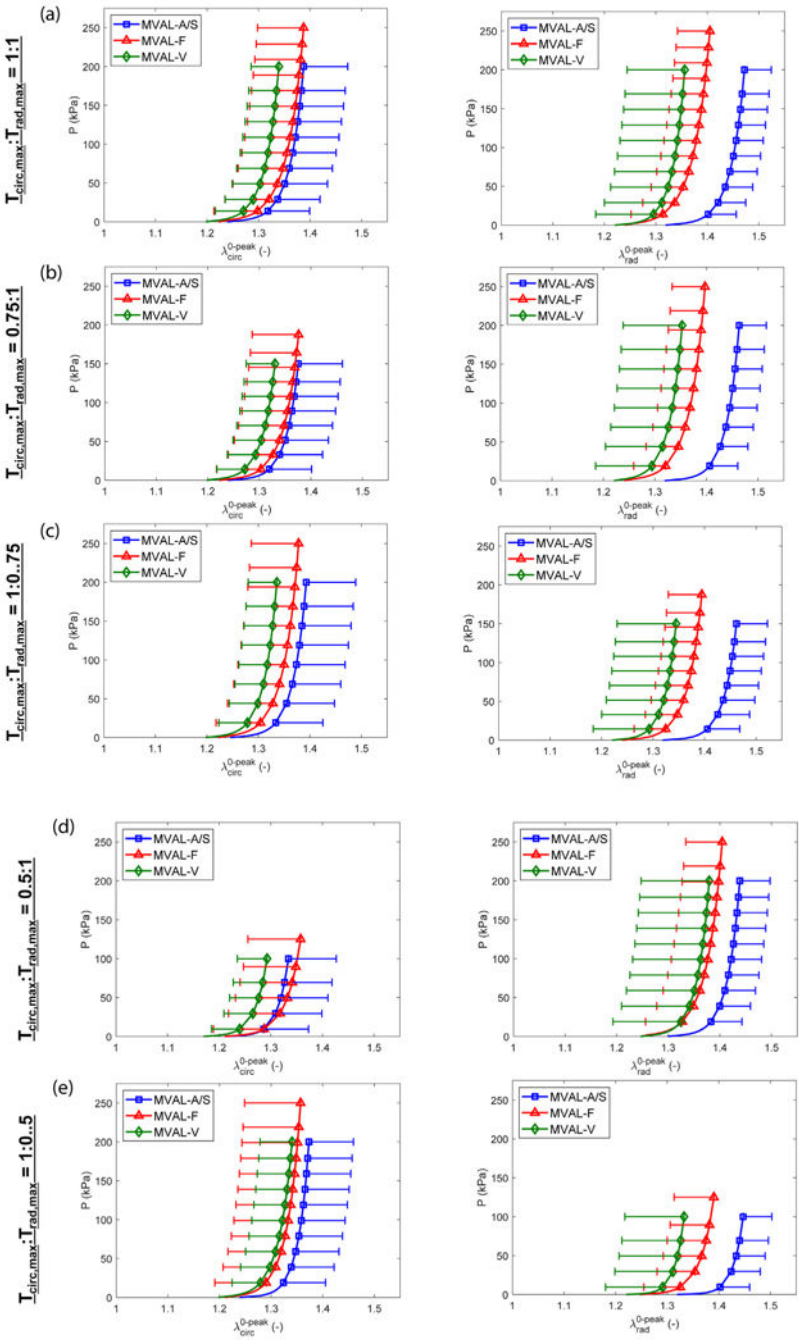

Fig. 8.

Mean ± SEM of the biaxial mechanical testing results (first Piola-Kirchhoff stress versus peak stretch) of MVAL layer tissues (n = 6) under five force-controlled loading protocols: $T_{circ,max}$:$T_{cird,max}$ = (a) 1:1, (b) 0.75:1, (c) 1:0.75, (d) 0.5:1, and (e) 1:0.5.

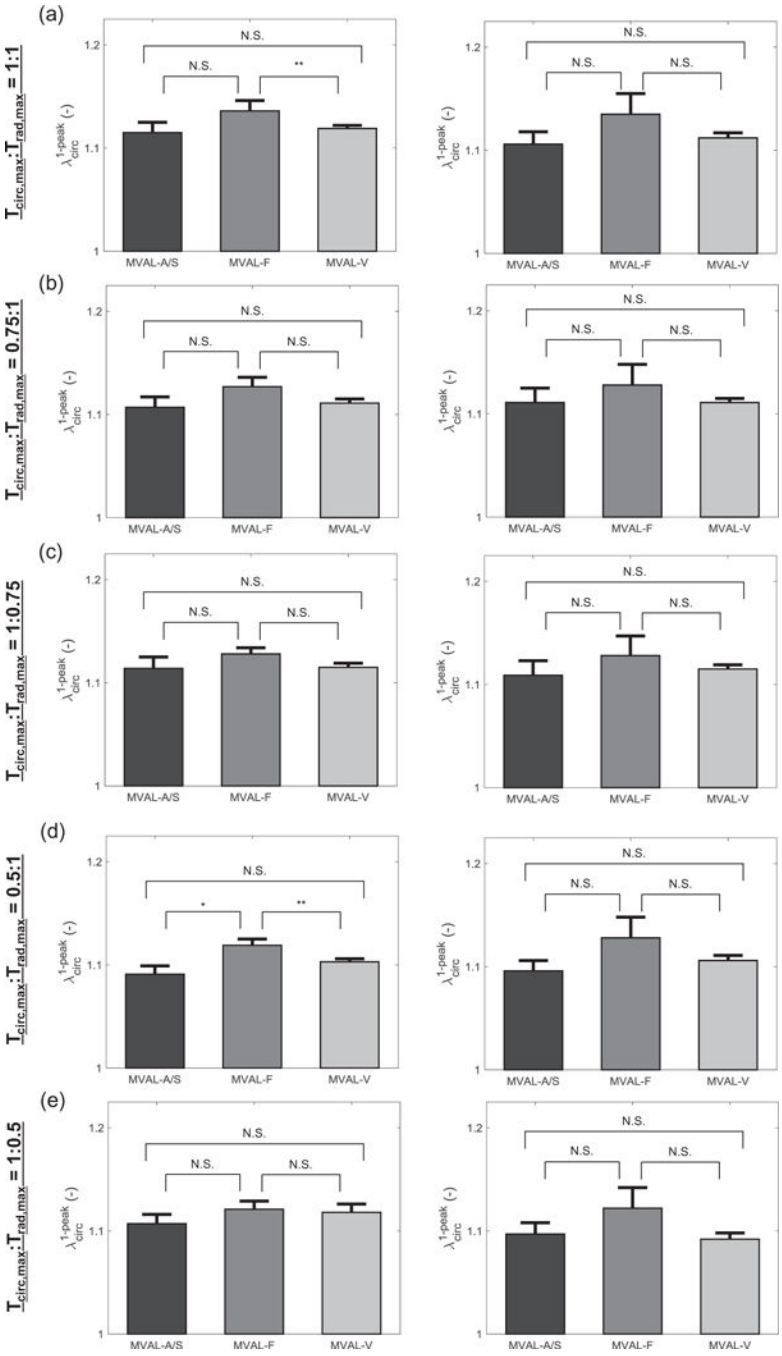

Fig. 9.

Comparisons of MVAL layer-specific mechanical stretches under five force-controlled loading protocols: $T_{circ,max}$:$T_{rad,max}$ = (a) 1:1, (b) 0.75:1, (c) 1:0.75, (d) 0.5:1, and (e) 1:0.5. (*) denotes statistically significant difference ($p < 0.05$) between layers, (**) denotes nearly statistically significant difference ($p < 0.1$) between layers, and (N.S.) denotes no statistically significant differences between the layers ($p > 0.1$).

Health Research Alliance Author Manuscript

Table 1

Comparison of the histologically-determined microstructural mass composition between the separated atrialis/spongiosa (A/S) and fibrosa/ventricularis (F/V) layers, and the intact TVAL tissue.

Tissue Specimen		A/S Layer	F/V Layer	Intact TVAL *
Thickness		0.33 mm	0.75 mm	1.08 mm
Mass Fraction	GAGs	44.6%	33.4%	27.4%
	Collagen	36.1%	52.1%	58.3%
	Elastin	19.3%	14.5%	14.3%

* The intact TVAL was not from the same tissue strip's section as the one used in analyses of the separated A/S, F, and V layers (cf. Section 2.5, Fig. 1b and Fig. 3c and d).

Health Research Alliance Author Manuscript

Table 2

Comparison of the microstructural mass compositions between the separated atrialis/spongiosa (A/S), fibrosa (F), and ventricularis (V) layers, and the intact MVAL tissue.

Tissue Specimen		A/S Layer	F Layer	V Layer	Intact MVAL*
Thickness		0.33 mm	0.92 mm	0.29 mm	0.94 mm
Thickness [8]		0.09 mm (20.1%)	0.32 mm (75.8%)	0.02 mm (4.1%)	0.42 mm
Mass Fraction	GAGs	30.2%	17.7%	21.6%	22.4%
	Collagen	34.8%	72.2%	49.9%	62.8%
	Elastin	35.0%	10.1%	28.5%	14.8%
Mass Fraction [8]	GAGs	38.4%	24.1%	13.6%	–
	Collagen	21.7%	67.1%	30.9%	–
	Elastin	39.9%	8.8%	55.5%	–

* The intact MVAL was not from the same tissue strip's section as the one used in in analyses of the separated A/S, F, and V layers (cf. Section 2.5, Fig. 1b and Fig. 3a and b).

Health Research Alliance Author Manuscript

Table 3

Peak tissue stretches and anisotropy index for MVAL and TVAL tissue layers (n = 6) under the equibiaxial loading protocol ($T_{circ,max}$:$T_{rad,max}$ = 1:1), together with the preconditioning stretches. All values are reported as mean ± SEM. In the statistical analysis the non-parametric Mann-Whitney *U* test was using comparing layers within the same valve leaflet.

	MVAL			**TVAL**	
	A/S	**F**	**V**	**A/S**	**F/V**
λ_{circ}^{0-peak}	1.38 ± 0.12	1.39 ± 0.12	1.34 ± 0.05	1.26 ± 0.05	1.17 ± 0.03
p-value	A/S vs. F: 0.937; A/S vs. V: 0.937; F vs. V: 0.937			A/S vs. F/V: 0.310	
λ_{rad}^{0-peak}	1.46 ± 0.05	1.41 ± 0.08	1.36 ± 0.11	1.37 ± 0.05	1.32 ± 0.08
p-value	A/S vs. F: 0.394; A/S vs. V: 0.104; F vs. V: 0.589			A/S vs. F/V: 0.310	
Anisotropy Index (AI)	1.09 ± 0.08	1.03 ± 0.04	1.01 ± 0.07	1.10 ± 0.05	1.12 ± 0.06
p-value	A/S vs. F: 0.589; A/S vs. V: 0.589; F vs. V: 1.000			A/S vs. F/V: 0.937	
λ_{circ}^{0-1}	1.24 ± 0.10	1.22 ± 0.10	1.20 ± 0.05	1.15 ± 0.05	1.06 ± 0.02
p-value	A/S vs. F: 0.818; A/S vs. V: 1.000; F vs. V: 0.818			A/S vs. F/V: 0.310	
λ_{rad}^{0-1}	1.32 ± 0.05	1.24 ± 0.08	1.22 ± 0.11	1.26 ± 0.05	1.20 ± 0.08
p-value	A/S vs. F: 0.485; A/S vs. V: 0.132; F vs. V: 0.589			A/S vs. F/V: 0.329	

Health Research Alliance Author Manuscript

Table 4

Mechanical stretches for MVAL and TVAL tissue layers (n = 6) under various biaxial mechanical loads. All values are reported as mean ± SEM. In the statistical analysis the non-parametric Mann-Whitney *U* test was using comparing layers within the same valve leaflet.

		MVAL			TVAL	
		A/S	**F**	**V**	**A/S**	**F/V**
$T_{circ,max}$: $T_{rad,max}$ = 1:1	λ_{circ}^{1-peak}	1.12 ± 0.01	1.14 ± 0.01	1.12 ± 3E–3	1.10 ± 0.01	1.11 ± 0.02
	p-value	A/S vs. F: 0.132; A/S vs. V: 0.310; F vs. V: 0.071			A/S vs. F/V: 0.818	
	λ_{rad}^{1-peak}	1.11 ± 0.01	1.14 ± 0.02	1.11 ± 0.01	1.09 ± 6E–3	1.10± 0.01
	p-value	A/S vs. F: 0.180; A/S vs. V: 0.394; F vs. V: 0.180			A/S vs. F/V: 0.790	
$T_{circ,max}$: $T_{rad,max}$ = 0.75.1	λ_{circ}^{1-peak}	1.11 ± 0.01	1.13 ± 0.01	1.11 ± 4E–3	1.10 ± 0.01	1.11 ± 0.02
	p-value	A/S vs. F: 0.132; A/S vs. V: 0.589; F vs. V: 0.180			A/S vs. F/V: 0.859	
	λ_{rad}^{1-peak}	1.11 ± 0.01	1.13 ± 0.02	1.11 ± 4E–3	1.09 ± 0.01	1.10 ± 0.01
	p-value	A/S vs. F: 0.485; A/S vs. V: 1.000; F vs. V: 0.236			A/S vs. F/V: 0.513	
$T_{circ,max}$: $T_{rad,max}$ = 1:0.75	λ_{circ}^{1-peak}	1.11 ± 0.01	1.13 ± 0.01	1.12 ± 4E–3	1.10 ± 0.01	1.11 ± 0.02
	p-value	A/S vs. F: 0.240; A/S vs. V: 0.513; F vs. V: 0.102			A/S vs. F/V: 0.513	
	λ_{rad}^{1-peak}	1.11 ± 0.01	1.13 ± 0.02	1.10 ± 0.01	1.09 ± 0.01	1.10 ± 0.01
	p-value	A/S vs. F: 0.394; A/S vs. V: 0.818; F vs. V: 0.132			A/S vs. F/V: 0.420	
$T_{circ,max}$: $T_{rad,max}$ = 0.5:1	λ_{circ}^{1-peak}	1.09 ± 0.01	1.12 ± 0.01	1.10 ± 3E–3	1.08 ± 0.01	1.10 ± 0.02
	p-value	A/S vs. F: 0.041; A/S vs. V: 0.180; F vs. V: 0.065			A/S vs. F/V: 0.331	
	λ_{rad}^{1-peak}	1.10 ± 0.01	1.13 ± 0.02	1.11 ± 0.01	1.09 ± 0.01	1.10 ± 0.01
	p-value	A/S vs. F: 0.240; A/S vs. V: 0.225; F vs. V: 0.121			A/S vs. F/V: 0.258	
$T_{circ,max}$: $T_{rad,max}$ = 1:0.5	λ_{circ}^{1-peak}	1.11 ± 0.01	1.12 ± 0.01	1.12 ± 0.01	1.10 ± 0.01	1.12 ± 0.02
	p-value	A/S vs. F: 0.258; A/S vs. V: 0.394; F vs. V: 0.818			A/S vs. F/V: 0.240	
	λ_{rad}^{1-peak}	1.10 ± 0.01	1.12 ± 0.02	1.09 ± 0.01	1.08 ± 4E–3	1.09 ± 0.01
	p-value	A/S vs. F: 0.394; A/S vs. V: 0.974; F vs. V: 0.104			A/S vs. F/V: 0.558	

Health Research Alliance Author Manuscript

Table 5

Statistical analysis results (p values) for comparing the circumferential and radial stretch values for a given layer considering different loading protocols.

		λ^{0-1}	$T_{circ,max}:T_{rad,max}=1:1$		$T_{circ,max}:T_{rad,max}=0.75:1$		$T_{circ,max}:T_{rad,max}=1:0.75$		$T_{circ,max}:T_{rad,max}=0.5:1$		$T_{circ,max}:T_{rad,max}=1:0.5$	
			λ^{0-peak}	λ^{1-peak}	λ^{0-peak}	λ^{1-peak}	λ^{0-peak}	λ^{1-peak}	λ^{0-peak}	λ^{1-peak}	λ^{0-peak}	λ^{1-peak}
TVAL	A/S	0.132	0.132	0.554	0.089	0.420	0.132	0.240	0.065	0.937	0.180	0.143
	F/V	0.093	0.310	0.327	0.180	0.974	0.310	0.513	0.180	0.619	0.310	0.065
MVAL	A/S	0.394	0.699	0.420	0.621	0.937	0.589	0.589	0.310	0.853	0.699	0.329
	F	0.699	0.589	0.818	0.589	0.818	0.589	0.818	0.515	0.699	0.589	0.619
	V	0.818	0.589	0.459	0.818	0.667	0.455	0.065	0.818	1.000	0.485	0.006